HIV transgene expression impairs K^+ channel function in the pulmonary vasculature

Gema Mondejar-Parreño[1,2], Daniel Morales-Cano[1,2], Bianca Barreira[1,2], María Callejo[1,2], Jesús Ruiz-Cabello[2,4], Laura Moreno[1,2], Sergio Esquivel-Ruiz[1,2], Alistair Mathie[3], Ghazwan Butrous[3], Francisco Perez-Vizcaino[1,2], Angel Cogolludo[1,2,#]

[1]Department of Pharmacology and Toxicology, School of Medicine, University Complutense of Madrid, Instituto de Investigación Sanitaria Gregorio Marañón (IiSGM), 28040 Madrid, [2]Ciber Enfermedades Respiratorias (CIBERES), Spain. [3]Medway School of Pharmacy. University of Kent and University of Greenwich. United Kingdom. [4]CIC biomaGUNE, 20014, Donostia-San Sebastián, Spain, IKERBASQUE, Basque Foundation for Science, Spain; and Universidad Complutense Madrid.

 # Corresponding author: Angel Cogolludo. Department of Pharmacology and Toxicology, School of Medicine, University Complutense of Madrid. Ciudad Universitaria S/N. 28040 Madrid. Spain.

Email: acogolludo@med.ucm.es

Phone: 0034913947120

Running head: K^+ channel dysfunction in HIV transgenic mice

Abstract

Human immunodeficiency virus (HIV) infection is an established risk factor for pulmonary arterial hypertension (PAH), however the pathogenesis of HIV-related PAH remains unclear. Since K^+ channel dysfunction is a common marker in most forms of PAH, our aim was to analyse if the expression of HIV proteins is associated with impairment of K^+ channel function in the pulmonary vascular bed. HIV transgenic mice (Tg26) expressing seven of the nine HIV viral proteins and wild type (Wt) mice were used. Hemodynamic assessment was performed by echocardiography and catheterization. Vascular reactivity was studied in endothelium-intact pulmonary arteries (PA). K^+ currents were recorded in freshly isolated PA smooth muscle cells (PASMC) using the patch-clamp technique. Gene expression was assessed using qRT-PCR. PASMC from Tg26 mice had reduced K^+ currents and were more depolarized that those from Wt. While Kv1.5 currents were preserved, pH-sensitive non-inactivating background currents (I_{KN}) were nearly abolished in PASMC from Tg26 mice. Tg26 mice had reduced lung expression of Kv7.1 and Kv7.4 channels and decreased responses to the Kv7.1 channel activator L634,373 assessed by vascular reactivity and patch-clamp experimental approaches. While we found pulmonary vascular remodeling and endothelial dysfunction in Tg26 mice, this was not accompanied by changes in hemodynamic parameters. In conclusion, the expression of HIV proteins *in vivo* impairs pH-sensitive I_{KN} and Kv7 currents. This negative impact of HIV proteins in K^+ channels, was not sufficient to induce PAH, at least in mice, but may play a permissive or accessory role in the pathophysiology of HIV-associated PAH.

Keywords: HIV, pulmonary hypertension, potassium channels, Kv7, TASK channels

INTRODUCTION

The human immunodeficiency virus (HIV) infection and its associated pathologies constitute a global health concern. It is estimated that around 37 million people are living with HIV globally (UNAIDS, 2017). Despite the success of highly active antiretroviral therapy, chronic inflammation persists and is independently associated with cardiovascular complications (44). Among the cardiovascular complications, HIV-associated pulmonary arterial hypertension (PAH) is especially severe and is associated with significant morbidity and mortality (4). Moreover, HIV patients have a 2500-fold increased risk of developing PAH and have a poorer prognosis than PAH in the general population (9). While only a small proportion (0.46%) of patients with HIV will develop HIV related PAH (42), there may be as many as 200,000 HIV-infected patients affected by PAH worldwide.

PAH is a complex disorder characterized by excessive vasoconstriction, inflammation and vascular remodeling that lead to reduced lumen of pulmonary arteries (PA) and increased pulmonary vascular resistance (34). The pathogenesis of PAH is rather multifactorial but impairment of K^+ channels is considered an early and common feature in most, if not all, forms of the disease (3, 34).

A variety of K^+ channels have been shown to play an essential role in controlling pulmonary vascular tone and their impairment results in a more depolarized membrane potential in PA smooth muscle cells (PASMC), leading to increased intracellular calcium, vasoconstriction and proliferation (3, 8). Dysfunction of K^+ channels, particularly the voltage-gated potassium channels-Kv Kv1.5 (encoded by *KCNA5*) (2-3, 31, 45) and the member of the two-pore domain potassium channel TWIK-related acid-sensitive potassium channel 1 (TASK-1, encoded by *KCNK3*) (1, 26, 37), have been found in experimental and clinical PAH and is considered a

contributing factor in the development of the disease (3, 37). During the last decade Kv7 (Kv7.1–Kv7.5) channels encoded by *KCNQ1–5* have emerged as key candidates to control vascular tone in several blood vessels, including the pulmonary circulation (6, 22, 24, 32). Interestingly, reduced *KCNQ4* expression has been reported in early phases of hypoxia-induced pulmonary hypertension (41) but this have not been consistently confirmed in other forms of the disease.

Although the mechanisms underpinning the pathophysiology of HIV-associated PAH remain still largely unknown, several HIV viral proteins have been proposed to contribute (4, 21). Thus, Nef, Tat and gp120 induce endothelial dysfunction (12, 23, 38) and have been proposed to initiate pulmonary vascular remodeling (4). Tat represses the transcription of the bone morphogenic protein receptor-2 (BMPR-2) (5), whose deficiency plays a key important role in the onset and progression of PAH (34). Vpu interacts with TASK-1 channels and disrupts its function (18) and expression of Nef has been associated with the development of complex pulmonary vascular lesions in simians (28). We hypothesized that the expression of HIV proteins is associated with impairment of K^+ channel function in the pulmonary circulation as occurs in other forms of PAH. To address this issue, we undertook experiments using the Tg26 transgenic non-infectious mice model which expresses seven of the nine proteins of the HIV.

MATERIALS AND METHODS

Animals. All experimental procedures utilizing animals were carried out according to the Spanish Royal Decree 1201/2005 and 53/2013 on the Care and Use of Laboratory Animals and approved by the institutional Ethical Committees of the Universidad Complutense de Madrid (Madrid, Spain) and the regional Committee for Laboratory Animals Welfare (Comunidad de

Madrid, Ref. number PROEXO-301/16). Age matched (10 weeks) male FVB/NJ (Wt) and HIV-1 transgenic mice on the FVB/NJ background (FVB/N-Tg(HIV)26Aln/PkltJ; Tg26) from the Jackson Laboratory (USA) were provided by Charles River (France). This HIV-1 Tg26 mice model express a transgene containing a portion of the HIV including Env and Tat, Nef, Rev, Vif, Vpr, and Vpu accessory genes but lacking part of the gag-pol region, rendering the virus non-infectious (11). Animals were kept under standard conditions of temperature 22±1°C and 12:12 hour dark/light cycle with free access to food and water.

Genotyping. Genomic DNA was isolated from tail biopsies of Wt and Tg26 mice with a lysis buffer of the following composition (in mmol/L): Tris.Cl ph8 10, EDTA 10, NaCl 100 and 0.5% SDS containing Proteinase K 0.1 in mg/mL for 16h at 55ºC. Then, genomic DNA was extracted with phenol/chloroform/isoamyl alcohol and purified. 100 ng of genomic DNA was used as template for standard PCR using the primers listed in Table 1 according to the genotyping protocol from The Jackson Laboratory.

Tissue and cell isolation. Resistance PA were carefully dissected free of surrounding tissue and cut into rings (1.8-2 mm length). For cell isolation, PA rings were cut into small segments and placed into a nominally Ca^{2+}-free physiological salt solution (PSS) of the following composition (in mmol/L): NaCl 130, KCl 5, MgCl 2 1.2, glucose 10, and HEPES 10 (pH 7.3 with NaOH) containing (in mg/mL) papain 1, dithiothreitol 0.8, and albumin 0.7 for 7-10 min. Thereafter, artery segments were incubated for an additional 3-5 min in Ca^{2+}-free PSS containing (in mg/mL) collagenase F 1, collagenase H 0.3, and albumin 0.7. PA smooth muscle cells (PASMC) were dissociated using a wide bore, smooth-tipped pipette. Cells were stored in Ca^{2+}-free PSS (4°C) and used within 8 h of isolation.

Recording of arterial reactivity. For contractile tension recording, PA rings were mounted in a wire myograph with Krebs buffer solution maintained at 37 °C and bubbled with 95 % O_2 and 5 % CO_2. Vessels were stretched to give an equivalent transmural pressure of 20 mmHg. Preparations were firstly stimulated by raising the K^+ concentration of the buffer (to $80x10^{-3}$ M) in exchange for Na^+. Vessels were washed three times and allowed to recover before a new stimulation. The relaxant effects induced by Acetylcholine (ACh, 10^{-9}-10^{-5} M), sodium nitroprusside (SNP, 10^{-11}-10^{-5} M) or Kv7 channel activators were examined in arteries stimulated with serotonin (5-HT, 10^{-5} M). Contraction induced by Kv1.5 or Kv7 channel inhibitors was assayed in the absence of pretone.

Electrophysiological studies. Membrane currents were recorded with an Axopatch 200B and a Digidata 1322A (Axon Instruments, Burlingame, CA, U.S.A) using the whole cell configuration of the patch-clamp technique. Total Kv currents were recorded following the application of 200 ms voltage steps ranging from -60 to +20 mV (7, 30). In some experiments long (4 s) depolarizing steps were applied in order to minimize the contribution of time-dependent delayed rectifier potassium currents (such as Kv1) and maximize the contribution of Kv7 currents as reported (32). Current-voltage relationships were constructed by measuring the currents at the end of the pulse. To record TASK-like currents, defined as the non-inactivating background K^+ current (I_{KN}), sensitive to pH, PASMC were clamped at 0 mV for 5 minutes to inactivate Kv channels and, subsequently, a 1s ramp from +60 mV to -100 mV was applied (16, 36) at pH 6.3 and 7.3. To minimize activation of BKCa channels cells were superfused with an external Ca^{2+}-free PSS (see above) and a Ca^{2+}-free pipette (internal) solution containing (mmol/L): KCl 110, $MgCl_2$ 1.2, Na_2ATP 5, HEPES 10, EGTA 10 (pH adjusted to 7.3 with KOH). Currents were normalized for cell capacitance and expressed in pA/pF as previously described (7, 30). All experiments were performed at room temperature.

PASMC culture. Primary PASMC obtained from intralobar PA explants and grown in Smooth Muscle Cell Growth Medium2 supplemented with Smooth Muscle Cell Growth Supplement (C-22062, PromoCell, Germany). The smooth muscle phenotype was confirmed by positive immunofluorescent staining using an anti-α-actin antibody (Sigma-Aldrich, Clone 1A4). PASMC between passages 1 or 2 were used for qRT-PCR studies.

qRT–PCR analysis. Total RNA was isolated and purified either from whole lung homogenates or from PASMC using the miRNEASY extraction kit according to manufacturer´s instructions (Qiagen, Hilden, Germany). Total RNA was reverse transcribed into cDNA using iScript TM cDNA Synthesis Kit (BioRad) following manufacturer's instructions. Real-time PCR was performed using a TaqMan system (Roche-Applied Biosystems, Mannheim, Germany) in the Genomic Unit of the Universidad Complutense de Madrid. Custom sense and anti-sense primers for *NOS3* and *BMPR2* with a Taqman probe number #56 (Roche, Cat: 04688538001) and # 67 (Roche, Cat: 0468866001), respectively and commercial primers from Applied Biosystems for *KCNA5, KCNK3, KCNQ1, KCNQ4, KCNQ5*, *NOS3*, *BMPR2* and *ACTB* expression were used (Table 1). The DDCt method was used to quantify mRNA. Target gene expression was normalized to the expression of *ACTB.*

Echocardiography. A two-dimensional motion-mode transthoracic echocardiography was performed at a frame rate above 230 frames/second using a Vevo 2100 system and a 30-MHz linear probe (Visualsonics, Toronto, Canada). Echocardiography examination was blindly performed by an expert operator. Colour and pulse wave (PW) Doppler were acquired with a pulse repetition frequency of 40 Kz to study pulmonary artery flows. PW Doppler was displayed just at the beginning of the pulmonary artery. The pulmonary acceleration time (PAT), ejection time (ET) and the ratio PAT/ET were measured to estimate right ventricular systolic pressure (43). Right ventricle systolic function was estimated using the tricuspid

annular plane systolic excursion (TAPSE) obtained from a d four-chamber apical view to measure maximum lateral tricuspid annulus motion. Mice were lightly anesthetized with 0.5-1.5% isoflurane in oxygen to maintain the heart rate along the experiments. Mice were positioned in supine position and kept in normothermia during the experiments with a heating platform and a warmed ultrasound gel.

Hemodynamic measurements. Mice were anesthetized i.p. with a mixture of 80 mg/kg ketamine (Mearial Lyon, France) plus 8 mg/kg xylacine (KVP Pharma und Veteriär-Produkte GmbH, Kiel, Germany). Before initiation of surgical procedure, general anesthesia was confirmed by assessing the absence of response to any stimulus. Then, animals were placed in a supine position on a thermostatically controlled electric heating blanket (Homeothemic Blanket Control Unit, Harvard Apparatus, March-Hugstetten, Germany) to maintain body temperature at 38°C. The tracheostomy was performed by a ventral neck incision followed by insertion of a 1.3-mm outer diameter tracheotomy cannula in the trachea. Animals were ventilated with room air (tidal volume 9 mL/Kg, 100 breaths/min, and a positive end-expiratory pressure of 2 cm H_2O) with a rodent ventilator (MiniVent Type 845, Harvard Apparatus, USA). After sternotomy, ventricular systolic pressure (RVSP), and systolic, diastolic and mean pulmonary arterial pressures (sPAP, dPAP and mPAP) were measured in open-chest mice as previously reported in rats (31). Measurements were recorded with a pressure transducer via a 0.7-mm internal diameter catheter (24 GA, BD Insyte, USA) introduced in the right ventricle and then advanced to the main PA.

Assessment of RV hypertrophy. At the end of the recordings, hearts were excised and the right ventricle (RV) and the left ventricle plus septum (LV+S) were carefully dissected and weighed. The Fulton index [RV/(LV+S)] and the ratio RV/body weight (BW) were calculated to assess right ventricular hypertrophy (31).

Lung histology. The right lung was inflated *in situ* with formol saline through the right bronchus and embedded in paraffin. Hematoxilyn and eosin staining and elastic Van Gieson (eVG) staining were performed in lung sections according to common histopathological procedures and examined by light microscopy. Small arteries (25–100 µm outer diameter) were analysed in a blinded fashion and categorized as muscular, partially muscular or nonmuscular as previously described (31). Medial wall thickness was defined by the area between the external elastic lamina and the internal elastic lamina marked by eVG staining. Around 500 representative vessels within a range of diameters from 20 to 70 µm were analyzed per sample.

Reagents. Drugs and reagents were obtained from Sigma-Aldrich Quimica (Spain), except retigabine (Axon, Groningen, The Netherlands) and L-364,373 (Tocris, Bristol, UK). Drugs were dissolved in DMSO and final vehicle concentrations were ≤ 0.1%.

Statistical analysis. Data are expressed as mean ± S.E.M.; n indicates the number of experiments from different animals, unless otherwise stated. Statistical analysis was performed using a Student's t-test for paired or unpaired observations, or one-way ANOVA followed by a Newman-Keuls test for multiple comparisons. When more than one sample came from the same animal, the nested ANOVA was applied. Differences were considered statistically significant when P was less than 0.05.

RESULTS

227 *Potassium channel dysfunction in PASMC from HIV-1 mice.* PASMC isolated from Tg26 mice had
228 similar membrane capacitance (20.3 ± 0.7 pF) compared to those isolated from Wt mice (19.7
229 ± 0.6 pF; $p > 0.05$). Figure 1A shows original traces of the total Kv currents recorded in
230 myocytes from both strains. Kv currents measured at the end of the 200 ms depolarizing
231 pulses were significantly smaller in PASMC from Tg26 mice than in those from Wt mice at
232 potentials more positive to -10 mV (Fig. 1B). Moreover, resting membrane potential was more
233 depolarized in PASMC from Tg26 mice than in those from wild type (Fig. 1C).

234

235 *Kv1.5 channels are not affected in PA from Tg26 mice.* We studied whether Kv1.5 currents,
236 which represent a main component of the total Kv current in the pulmonary vasculature (30),
237 were affected in Tg26 mice. We found that the selective Kv1.5 channel inhibitor DPO-1 (10^{-6} M)
238 induced a marked reduction of the Kv currents in both Wt- (Fig. 2A) and Tg26- (Fig. 2B) derived
239 PASMC. Thus, DPO-1-sensitive currents, which reflect the Kv1.5 channel component, were not
240 significantly different in both cell types (Fig. 2C). In addition, DPO-1 had negligible effects on
241 vascular tone in arteries isolated from both strains (Fig. 2D and E). In line with these data, the
242 gene encoding for Kv1.5 (*KCNA5*) was similarly expressed in lungs (Fig. 2F) or PASMC (Fig. 2G)
243 isolated from both strains. These data suggested that K^+ channels, other than Kv1.5, were
244 impaired in PA from Tg26 mice.

245

246 *PH-sensitive I_{KN} currents are impaired in PA from HIV-1 Tg26 mice.* Fig. 3A shows original
247 recordings of I_{KN} at different pH during the application of voltage ramps from 60 to −100 mV
248 from a holding potential of 0 mV. In Wt PASMC I_{KN} was inhibited when switching the pH of the
249 external solution from 7.3 to 6.3. The I-V relation of the pH-sensitive current yielded a non-
250 voltage-gated current as expected for TASK-like currents (Fig. 3B). On the other hand, currents

from Tg26 mice were not inhibited by extracellular acidification (Fig. 3A and B). In addition, acidification led to membrane depolarization in Wt (Fig. 3D) but not in Tg26 (Fig. 3E) PASMC. Thus, both pH-sensitive K^+ current (Fig. 3C) and pH-induced depolarization (Fig. 3F) were markedly attenuated in cells from Tg26 mice. These differences were unrelated to changes in the expression of *KCNK3* in lungs or PASMC (Fig. 3G and H). Consistent with previous reports (35), we were unable to analyze TASK-1, the protein encoded by *KCNK3*, in lung samples because commercially available antibodies did not identify the protein in the Western blots.

Kv7 channels are impaired in PA from HIV-1 Tg26 mice. The non-inactivating voltage-gated Kv7 currents were studied by applying long (4 s) depolarizing pulses as previously reported (32). The K^+ current measured at the end of these pulses was diminished in PASMC from Tg26 mice (Fig. 4A and B). To further characterize the role of Kv7 channels, cells were exposed to the selective Kv7 channel inhibitor XE991. At $3x10^{-7}$ M, this drug reduced the current in Wt- (Fig. 4A and 4C) but not in Tg26- (Fig. 4A and D) derived PASMC. Thus, the current sensitive to XE991 was abrogated in PASMC from Tg26 mice (Fig. 4E). In PA isolated from Wt mice XE991 ($3x10^{-6}$ M) elicit a robust contraction that was significantly smaller in PA from Tg26 mice (Fig. 4F and G). Similar results were obtained with linopirdine (10^{-5} M), another Kv7 channel inhibitor (Fig. 4H). Quantitative analysis of mRNA expression of specific genes encoding for the most predominant Kv7 channels (Kv7.1, Kv7.4 and Kv7.5) in the vascular bed revealed a reduced expression of *KCNQ1* and *KCNQ4*, but not *KCNQ5* (Fig. 5A), in lungs from Tg26 as compared to Wt mice. Thus we assessed the effects of L-364,373 which selectively activates Kv7.1 channels and retigabine that activates Kv7.2 through Kv7.5 channels. The addition of L634,373 led to an enhancement of the current in PASMC from Wt but not from Tg26 and (Fig. 5B and C). On the other hand, retigabine had no effect on the current in either cell type (Fig. 6A and B). We also analysed the relaxant responses induced by both drugs. The relaxation

induced by L-364,373 was significantly reduced in PA from Tg26 mice (Fig. 5D and E). However, no differences were found in the relaxant responses induced by retigabine between both Wt and Tg26 PA (Fig. 6C and D).

Assessment of pulmonary hemodynamics and remodeling. Table 2 summarizes the hemodynamic parameters obtained by Doppler echocardiography in Wt and HIV-1 Tg26 mice. PAT, ET, PAT/ET and TAPSE values were similar in both strains. Fig. 7A shows original recordings of pulmonary arterial pressure by PA catheterization. In line with the echocardiography findings no differences were found in pulmonary hemodynamics (dPAP, sPAP and mPAP, Fig. 7B), RVSP (Fig. 7C) or heart rate (Fig. 7D) assessed by catheterization. The assessment on cardiac remodeling by the fulton index (RV/S+LV, Fig. 7E) or RV/body weight (Fig. 7F) revealed no significant right ventricular hypertrophy in Tg26 compared to Wt.

PA from HIV-1 Tg26 exhibit endothelial dysfunction. Contractile responses induced by KCl and 5-HT were similar in PA isolated from both Tg26 and Wt mice (Fig. 8A-C). We then analyzed the relaxation induced by the nitric oxide-cGMP pathway in 5-HT contracted arteries. The relaxation induced by ACh (endothelial dependent; Fig. 8D), but not that of SNP (endothelial independent, Fig. 8E), was attenuated in PA from Tg26 mice. This endothelial dysfunction was not associated with changes in the expression of genes encoding for eNOS (*NOS3*) or BMPR2 (*BMPR2*) (Fig. 8G and H). We also assessed the endothelial-mediated relaxation in mesenteric arteries. Although there was a trend for reduced relaxation in mesenteric arteries from Tg26, differences did not reach statistical significance (Fig. 8F).

299 Fig. 9A shows representative images of hematoxylin and eosin stained lung sections from Wt
300 and HIV-1 Tg26 mice. Pulmonary arteries were classified into non muscular, partially muscular
301 and muscular arteries (Fig. 9B). A modest vascular remodeling consisting of an increased
302 percentage of partially muscular and muscular PA and decreased percentage of non-muscular
303 PA was observed in Tg26 mice. Moreover, a significant increase in medial wall thickness,
304 assessed by the elastic Van Gieson staining, was found in Tg26 as compared to Wt mice (Fig. 9C
305 and D).
306
307

DISCUSSION

In the present study we report that HIV transgene expression leads to attenuation of endothelial-dependent relaxation and impairment of K^+ channel activity in the pulmonary vasculature. In particular, a marked reduction of pH-sensitive I_{KN} and Kv7 currents was found in PASMC from mice expressing HIV proteins. Our study identifies novel pathogenic factors that could play a role in the development of PAH associated to HIV. This is the first study reporting K^+ channel dysfunction by HIV in the pulmonary circulation.

With the advent of combination antiretroviral therapy, HIV-associated comorbidities like cardiovascular diseases have become a leading cause of death in HIV infected patients. Among them, PAH is a life-threatening complication of HIV infection (4). The mechanisms involved in the pathogenesis of HIV-PAH are not completely understood but HIV proteins such as Gp120, Tat, and Nef are considered candidate contributors (4, 21). Thus, to get insight into the mechanisms involved in PAH associated to HIV we took advantage of a transgenic mice expressing seven of the nine HIV proteins.

Our non-invasive (by echocardiography) and invasive (by PA catheterization) hemodynamic assessments revealed that pulmonary arterial pressures were not elevated in Tg26 mice. Accordingly, we found no changes in right ventricular weight. Previous studies in HIV transgenic rats have shown elevated PA pressure and right ventricular hypertrophy (25, 29); while other study by Porter et al (40) showed that Fischer 344 rats expressing HIV proteins were normotensive, even though these animals had exacerbated PAH in response to hypoxic exposure. In comparison with these studies, animals used in our study were much younger (10

weeks versus 4-9 months) so we cannot rule out that these animals may develop PAH at older ages. But most likely the lack of PAH in HIV Tg26 mice can be attributed to the notable differences in the development of this disease between rat and mice (15). These include, among others, the development of less PA thickening and PH in mice than rats after chronic hypoxia, or the induction of reversible (in mice) versus non-reversible and fatal (in rats) PH induced by the exposition to SU5416/hypoxia (15). These data strongly suggest that the expression of HIV-1 may predispose, but appears insufficient, to induce PAH in the mouse model. Noteworthy, the majority of patients with HIV infection are also not affected of PAH. Albeit HIV-1 Tg26 mice had PA pressures similar to Wt mice, we observed changes characteristic of PAH such as pulmonary vascular remodeling, endothelial dysfunction, and K^+ channel impairment. Likewise, severe pulmonary arterial muscularization can occur in mice without the development of PAH or RV hypertrophy (10). We also found that PA from HIV-1 Tg26 mice had endothelial dysfunction as demonstrated by attenuated relaxation to ACh with unaffected relaxation to SNP. Whilst similar results have been observed in large systemic arteries from HIV-1 transgenic mice (17), in our study the endothelial-dependent vasodilation was not impaired in mesenteric arteries. Several mechanisms have been proposed to account for the endothelial dysfunction in systemic arteries from HIV-associated PAH including the downregulated *BMPR2* or *NOS3* gene expression (5, 12, 23, 38). However, we found unaltered *BMPR2* or *NOS3* expression in lungs from Tg26 mice. Alternative mechanisms proposed for HIV-1-induced endothelial dysfunction, which we did not further explore, include increased production of reactive oxygen species and accelerated NO degradation (19-20) or increased levels of asymmetric dimethylarginine (ADMA) which competitively inhibits eNOS activity (39).

K^+ channels play a central role in governing membrane potential in PASMC and their impairment is associated with depolarization, increased vasoconstriction and proliferation (3,

8, 37). Our experiments demonstrate that total K^+ currents are attenuated in PASMC from HIV-1 Tg26 mice and this is associated with a more depolarized resting membrane potential. Among the different K^+ channels expressed in PASMC, special attention has been given to Kv1.5 and TASK-1 channels due to their role in controlling pulmonary vascular tone and in the pathogenesis of PAH. Reduced expression and function of Kv1.5 channels is a common characteristic in many forms of human and experimental PAH (2-3, 31, 45). Similarly, Lund et al (25) found that expression of *KCNA5*, the gene encoding for Kv1.5 channels, is reduced in lungs from HIV-1 transgenic rats that exhibit pulmonary hypertension. Herein, we comparatively analyzed the expression and activity (using the selective inhibitor DPO-1) of Kv1.5 channels in both Wt vs HIV-1 Tg26 mice. We found that DPO-1 exerted similar effects on total Kv current and contraction in both strains strongly suggesting a similar contribution of Kv1.5 channels. Intriguingly, DPO-1 sensitive current in PASMC from Tg26 mice reached an apparent plateau at positive potentials, which could be due to the partial contribution of residual BKCa current. Likewise, no differences were found in *KCNA5* expression in lungs or PASMC from Wt vs Tg26 mice. The reason for the discrepancies between our and Lund´s study is unknown but may rely on different animal species used. Another possible explanation is that downregulation of *KCNA5* is secondary to the development of PH, as occurred in the referred study.

There is compelling evidence that impairment of TASK-1 channels (encoded by *KCNK3*), a member of the two-pore domain background potassium channels family, plays a role in PAH (3, 37). Thus, the association between loss of function of *KCNK3* and PAH has been identified in hereditary and other forms of the disease (1, 26, 37). However, its role in PAH associated to HIV-1 remains unknown. A distinguishing feature of TASK channels is their pH dependence, thus we aimed to compare the activity of TASK channels in Wt and Tg26 mice by examining the acid-sensitivity of the background current I_{KN}. In PASMC from Wt we found that acidification of

extracellular pH inhibited the I_{KN} current leading to membrane depolarization, suggesting a functional role of TASK-like channels. These results are in line with previous data in rat (14), rabbit (16) or human (36) PASMC, albeit this pH sensitive current was not observed in a previous study in mouse PASMC (27). In contrast to what we observed in Wt cells, PASMC from Tg26 mice were essentially insensitive to pH. The mechanism underlying the reduced pH-sensitive current in HIV-1 expressing mice remains unknown, but it is tempting to speculate a role of the HIV-1 accessory protein Vpu. It is worth highlighting that Vpu shares structural homology with the N-terminal region of the TASK channel family members, including TASK-1, and that Vpu and TASK-1 oligomerize in vitro and in lymphoid tissues from AIDS patients (18). Moreover, the coexpression of Vpu and TASK-1 in heterologous systems leads to the suppression of the TASK current. Conversely, overexpression of TASK-1 suppresses HIV-1 replication (13). However, we could not confirm the protein expression of Vpu in the lung (with a commercially available antibody, ab81532).

Findings from the last years suggest that Kv7 channels are key regulators of vascular tone and reduced expression and activity of Kv7 channels has been reported in several cardiovascular diseases including essential hypertension (6, 22) or diabetes (32). Kv7 channels make also an important contribution on the regulation of pulmonary vascular tone (24). Moreover, the vascular responses to Kv7 channel modulators are depressed in two murine models of pulmonary hypertension (33) suggesting a Kv7 channel impairment. In fact, reduced *KCNQ4* expression has been noticed in PA from rats exposed to hypoxia for 3 days, which corresponds to the onset of pulmonary hypertension development (41). Herein, we dissected the Kv7 non-inactivating voltage-gated K^+ currents by applying long depolarizing pulses and by the use of Kv7.1-7.5 channel blocker XE991. The amplitude of this Kv7 current was markedly reduced in PASMC from Tg26 mice. Accordingly, XE991 as well as another Kv7 channel blocker linopirdine

elicited greater vasoconstrictor responses in PA from Wt than from Tg26. To ascertain if these differences were related to loss of channel expression in Tg26 lungs we analyzed the gene expression of the most relevant Kv7 channels in the vasculature. Our data confirmed a reduced expression of *KCNQ1* and *KCNQ4*, but not *KCNQ5* in lungs from HIV-1 Tg26. We also tested the effects of the selective Kv7.1 activator L364,373 and retigabine (which activates Kv7.2 through Kv7.5). We observed that the electrophysiological and relaxant effects of L364,373 were reduced in PASMC from HIV-1 Tg26, while retigabine did not enhance the currents and had comparable relaxation in PA from both strains. Altogether, our data indicate that Kv7 channel (especially Kv7.1) activity and expression is impaired in mice expressing HIV-1 proteins.

In conclusion, we demonstrate that the expression of HIV proteins *in vivo* impairs TASK-like and Kv7 channel activities but preserves Kv1.5 channel currents. Decreased Kv7 currents can be explained by downregulated gene expression of the channel and was functionally correlated with reduced vasodilation to a Kv7.1 channel activator. This negative impact of HIV proteins in pulmonary K^+ channels, was not sufficient to induce PAH, at least in mice, but may play a permissive or accessory role in the pathophysiology of HIV-associated PAH.

GRANTS

This work was supported by grants and fellowships by the Spanish Ministerio de Economia y Competitividad (SAF2014-55399-R and SAF2016-77222-R to AC and to FP-V; and SAF2017-84494-C2-1R to JR-C), Instituto de Salud Carlos III (PI15/01100 to LM), with funds co-financed by ERDF (FEDER) Funds from the European Commission, "A way of making Europe", and the Cardiovascular Medical Research and Education Fund (AC and GB) and Fundación Contra la Hipertensión Pulmonar-EMPATHY. G.M.P, M.C. and S.E.R. are funded by CIBERES, Universidad Complutense and FPU grants, respectively.

DISCLOSURES

No conflicts of interest, financial or otherwise, are declared by the authors.

AUTHOR CONTRIBUTIONS

A.C., G.B., F.P.V. and A.M. conceived and designed research; G.M.P., D.M.C., B.B., M.C. and S.E.R. performed experiments; G.M.P., D.M-C., B.B., M.C and A.C analyzed data; A.C., F.P.V., L.M., A.M., G.M.P., D.M.C, and J.R.C. interpreted results of experiments; A.C., G.M.P, D. M.C. and B.B. prepared figures; A.C. drafted manuscript; A.C., G.M.P., D.M.C., L.M., A.M., G.B. and F.P.V. edited and revised manuscript; All authors approved final version of manuscript.

ACKNOWLEDGMENTS

Authors thank Djuro Kosanovic, Christina Vroom and Ewa Bieniek for technical assistance and for the loan of their equipment on the Excellence Cluster Cardiopulmonary System, University of Giessen and Marburg Lung Center (UGMLC).

References

1. **Antigny F, Hautefort A, Meloche J, Belacel-Ouari M, Manoury B, Rucker-Martin C, Péchoux C, Potus F, Nadeau V, Tremblay E, Ruffenach G, Bourgeois A, Dorfmüller P, Breuils-Bonnet S, Fadel E, Ranchoux B, Jourdon P, Girerd B, Montani D, Provencher S, Bonnet S, Simonneau G, Humbert M, Perros F.** Potassium channel subfamily K member 3 (KCNK3) contributes to the development of pulmonary arterial hypertension. *Circulation* 133: 1371-1385, 2016. doi: 10.1161/CIRCULATIONAHA.115.020951.
2. **Bonnet S, Michelakis ED, Porter CJ, Andrade-Navarro MA, Thebaud B, Haromy A, Harry G, Moudgil R, McMurtry MS, Weir EK, Archer SL**. An abnormal mitochondrial-hypoxia inducible factor-1alpha-Kv channel pathway disrupts oxygen sensing and triggers pulmonary arterial hypertension in fawn hooded rats: similarities to human pulmonary arterial hypertension. *Circulation* 113: 2630-2641, 2006.
3. **Boucherat O, Chabot S, Antigny F, Perros F, Provencher S, Bonnet S.** Potassium channels in pulmonary arterial hypertension. Eur Respir J. 2015 Oct;46(4):1167-77. doi: 10.1183/13993003.00798-2015.
4. **Butrous G.** Human immunodeficiency virus-associated pulmonary arterial hypertension: considerations for pulmonary vascular diseases in the developing world. *Circulation* 131:1361-1370, 2015. doi: 10.1161/CIRCULATIONAHA.114.006978.
5. **Caldwell RL, Gadipatti R, Lane KB, Shepherd VL.** HIV-1 TAT represses transcription of the bone morphogenic protein receptor-2 in U937 monocytic cells. *J Leukoc Biol* 79: 192-201, 2006.
6. **Chadha PS, Zunke F, Zhu HL, Davis AJ, Jepps TA, Olesen SP, Cole WC, Moffatt JD, Greenwood IA.** Reduced KCNQ4-encoded voltage dependent potassium channel activity underlies impaired β-adrenoceptor mediated relaxation of renal arteries in hypertension. *Hypertension* 59: 877-884, 2012. doi: 10.1161/HYPERTENSIONAHA.111.187427.

7. **Cogolludo A, Moreno L, Lodi F, Frazziano G, Cobeño L, Tamargo J, Perez-Vizcaino F.** Serotonin inhibits voltage-gated K+ currents in pulmonary artery smooth muscle cells: role of 5-HT2A receptors, caveolin-1, and Kv1.5 channel internalization. *Circ Res* 98: 931-938, 2006.
8. **Cogolludo A, Moreno L, Villamor E.** Mechanisms controlling vascular tone in pulmonary arterial hypertension: implications for vasodilator therapy. *Pharmacology* 79: 65-75, 2007.
9. **Correale M, Palmiotti GA, Lo Storto MM, Montrone D, Foschino Barbaro MP, Di Biase M, Lacedonia D.** HIV-associated pulmonary arterial hypertension: from bedside to the future. *Eur J Clin Invest* 45: 515-28, 2015. doi: 10.1111/eci.12427.
10. **Daley E, Emson C, Guignabert C, de Waal Malefyt R, Louten J, Kurup VP, Hogaboam C, Taraseviciene-Stewart L, Voelkel NF, Rabinovitch M, Grunig E, Grunig G.** Pulmonary arterial remodeling induced by a Th2 immune response. *J Exp Med* 205: 361-72, 2008. doi: 10.1084/jem.20071008.
11. **Dickie P, Felser J, Eckhaus M, Bryant J, Silver J, Marinos N, Notkins AL.** HIV-associated nephropathy in transgenic mice expressing HIV-1 genes. *Virology* 185: 109-19, 1991.
12. **Duffy P, Wang X, Lin PH, Yao Q, Chen C.** HIV Nef protein causes endothelial dysfunction in porcine pulmonary arteries and human pulmonary artery endothelial cells. *J Surg Res* 156: 257-264, 2009. doi: 10.1016/j.jss.2009.02.005.
13. **Emeagwali N, Hildreth JE.** Human immunodeficiency virus type 1 Vpu and cellular TASK proteins suppress transcription of unintegrated HIV-1 DNA. *Virol* J 9: 277, 2012. doi: 10.1186/1743-422X-9-277.
14. **Gardener MJ, Johnson IT, Burnham MP, Edwards G, Heagerty AM, Weston AH.** Functional evidence of a role for two-pore domain potassium channels in rat mesenteric and pulmonary arteries. *Br J Pharmacol* 142: 192-202, 2004.
15. **Gomez-Arroyo J, Saleem SJ, Mizuno S, Syed AA, Bogaard HJ, Abbate A, Taraseviciene-Stewart L, Sung Y, Kraskauskas D, Farkas D, Conrad DH, Nicolls MR, Voelkel NF.** A brief

499 overview of mouse models of pulmonary arterial hypertension: problems and prospects.
500 *Am J Physiol Lung Cell Mol Physiol* 302: L977-L991, 2012. doi: 10.1152/ajplung.00362.2011.
501 16. **Gurney AM, Osipenko ON, MacMillan D, McFarlane KM, Tate RJ, Kempsill FE.** Two-pore
502 domain K channel, TASK-1, in pulmonary artery smooth muscle cells. *Circ Res* 93: 957-964,
503 2003.
504 17. **Hansen L, Parker I, Sutliff RL, Platt MO, Gleason RL Jr.** Endothelial dysfunction, arterial
505 stiffening, and intima-media thickening in large arteries from HIV-1 transgenic mice. *Ann*
506 *Biomed Eng* 41: 682-693, 2013. doi: 10.1007/s10439-012-0702-5.
507 18. **Hsu K, Seharaseyon J, Dong P, Bour S, Marbán E.** Mutual functional destruction of HIV-1
508 Vpu and host TASK-1 channel. *Mol Cell* 14: 259-267, 2004.
509 19. **Ivanov AV, Valuev-Elliston VT, Ivanova ON, Kochetkov SN, Starodubova ES, Bartosch B,**
510 **Isaguliants MG.** Oxidative stress during HIV infection: mechanisms and consequences.
511 *Oxid Med Cell Longev* 2016:8910396, 2016.
512 20. **Jacob BA, Porter KM, Elms SC, Cheng PY, Jones DP, Sutliff RL.** HIV-1-induced pulmonary
513 oxidative and nitrosative stress: exacerbated response to endotoxin administration in HIV-
514 1 transgenic mouse model. *Am J Physiol Lung Cell Mol Physiol* 291: L811-L819, 2006.
515 21. **Jarrett H, Barnett C.** HIV-associated pulmonary hypertension. *Curr Opin HIV AIDS* 12: 566-
516 571, 2017. doi: 10.1097/COH.0000000000000418.
517 22. **Jepps TA, Chadha PS, Davis AJ, Harhun MI, Cockerill GW, Olesen SP, Hansen RS,**
518 **Greenwood IA.** Downregulation of Kv7.4 channel activity in primary and secondary
519 hypertension. *Circulation* 124: 602-611, 2011. doi: 10.1161/CIRCULATIONAHA.111.032136.
520 23. **Jiang J, Fu W, Wang X, Lin PH, Yao Q, Chen C.** HIV gp120 induces endothelial dysfunction
521 in tumour necrosis factor-α-activated porcine and human endothelial cells. *Cardiovasc Res*
522 87: 366-374, 2010. doi: 10.1093/cvr/cvq013.

24. **Joshi S, Sedivy V, Hodyc D, Herget J, Gurney AM.** KCNQ modulators reveal a key role for KCNQ potassium channels in regulating the tone of rat pulmonary artery smooth muscle. *J Pharmacol Exp Ther* 329: 368-376, 2009. doi: 10.1124/jpet.108.147785.

25. **Lund AK, Lucero J, Herbert L, Liu Y, Naik JS.** Human immunodeficiency virus transgenic rats exhibit pulmonary hypertension. *Am J Physiol Lung Cell Mol Physiol* 301: L315-L326, 2011. doi: 10.1152/ajplung.00045.2011.

26. **Ma L, Roman-Campos D, Austin ED, Eyries M, Sampson KS, Soubrier F, Germain M, Trégouët DA, Borczuk A, Rosenzweig EB, Girerd B, Montani D, Humbert M, Loyd JE, Kass RS, Chung WK.** A novel channelopathy in pulmonary arterial hypertension. *N Engl J Med* 369: 351-361, 2013. doi: 10.1056/NEJMoa1211097.

27. **Manoury B, Lamalle C, Oliveira R, Reid J, Gurney AM.** Contractile and electrophysiological properties of pulmonary artery smooth muscle are not altered in TASK-1 knockout mice. *J Physiol* 589: 3231-3246, 2011. doi: 10.1113/jphysiol.2011.206748.

28. **Marecki JC, Cool CD, Parr JE, Beckey VE, Luciw PA, Tarantal AF, Carville A, Shannon RP, Cota-Gomez A, Tuder RM, Voelkel NF, Flores SC.** HIV-1 Nef is associated with complex pulmonary vascular lesions in SHIV-nef-infected macaques. *Am J Respir Crit Care Med* 174: 437-445, 2006.

29. **Mermis J, Gu H, Xue B, Li F, Tawfik O, Buch S, Bartolome S, O'Brien-Ladner A, Dhillon NK.** Hypoxia-inducible factor-1 α/platelet derived growth factor axis in HIV-associated pulmonary vascular remodeling. *Respir Res* 12: 103, 2011. doi: 10.1186/1465-9921-12-103.

30. **Moral-Sanz J, Gonzalez T, Menendez C, David M, Moreno L, Macias A, Cortijo J, Valenzuela C, Perez-Vizcaino F, Cogolludo A.** Ceramide inhibits Kv currents and contributes to TP-receptor-induced vasoconstriction in rat and human pulmonary arteries. *Am J Physiol Cell Physiol* 301: C186-C194, 2011. doi: 10.1152/ajpcell.00243.2010.

31. **Morales-Cano D, Menendez C, Moreno E, Moral-Sanz J, Barreira B, Galindo P, Pandolfi R, Jimenez R, Moreno L, Cogolludo A, Duarte J, Perez-Vizcaino F.** The flavonoid quercetin

549 reverses pulmonary hypertension in rats. *PLoS One* 9: e114492, 2014. doi:
550 10.1371/journal.pone.0114492.
551 32. **Morales-Cano D, Moreno L, Barreira B, Pandolfi R, Chamorro V, Jimenez R, Villamor E,**
552 **Duarte J, Perez-Vizcaino F, Cogolludo A.** Kv7 channels critically determine coronary artery
553 reactivity: left-right differences and down-regulation by hyperglycaemia. *Cardiovasc Res*
554 106: 98-108, 2015. doi: 10.1093/cvr/cvv020.
555 33. **Morecroft I, Murray A, Nilsen M, Gurney AM, MacLean MR.** Treatment with the Kv7
556 potassium channel activator flupirtine is beneficial in two independent mouse models of
557 pulmonary hypertension. *Br J Pharmacol* 157: 1241-1249, 2009. doi: 10.1111/j.1476-
558 5381.2009.00283.x.
559 34. **Morrell NW, Adnot S, Archer SL, Dupuis J, Jones PL, MacLean MR, McMurtry IF, Stenmark**
560 **KR, Thistlethwaite PA, Weissmann N, Yuan JXJ, Weir EK.** Cellular and molecular basis of
561 pulmonary arterial hypertension. *J Am Coll Cardiol* 54 (1 Suppl): S20–S31, 2009. doi:
562 10.1016/j.jacc.2009.04.018.
563 35. **Murtaza G, Mermer P, Goldenberg A, Pfeil U, Paddenberg R, Weissmann N, Lochnit G,**
564 **Kummer W.** TASK-1 potassium channel is not critically involved in mediating hypoxic
565 pulmonary vasoconstriction of murine intra-pulmonary arteries. PLoS One 12: e0174071,
566 2017. doi: 10.1371/journal.pone.0174071.
567 36. **Olschewski A, Li Y, Tang B, Hanze J, Eul B, Bohle RM, Wilhelm J, Morty RE, Brau ME, Weir**
568 **EK, Kwapiszewska G, Klepetko W, Seeger W, Olschewski H.** Impact of TASK-1 in human
569 pulmonary artery smooth muscle cells. *Circ Res* 98: 1072-1080, 2006.
570 37. **Olschewski A, Veale EL, Nagy BM, Nagaraj C, Kwapiszewska G, Antigny F, Lambert M,**
571 **Humbert M, Czirják G, Enyedi P, Mathie A.** TASK-1 (KCNK3) channels in the lung: from cell
572 biology to clinical implications. *Eur Respir J* 50: pii: 1700754, 2017. doi:
573 10.1183/13993003.00754-2017.

38. **Paladugu R, Fu W, Conklin BS, Lin PH, Lumsden AB, Yao Q, Chen C.** HIV Tat protein causes endothelial dysfunction in porcine coronary arteries. *J Vasc Surg* 38: 549-555, 2003.

39. **Parikh RV, Scherzer R, Nitta EM, Leone A, Hur S, Mistry V, Macgregor JS, Martin JN, Deeks SG, Ganz P, Hsue PY.** Increased levels of asymmetric dimethylarginine are associated with pulmonary arterial hypertension in HIV infection. *AIDS* 28: 511-519, 2014. doi: 10.1097/QAD.0000000000000124.

40. **Porter KM, Walp ER, Elms SC, Raynor R, Mitchell PO, Guidot DM, Sutliff RL.** Human immunodeficiency virus-1 transgene expression increases pulmonary vascular resistance and exacerbates hypoxia-induced pulmonary hypertension development. *Pulm Circ* 3: 58-67, 2013. doi: 10.4103/2045-8932.109915.

41. **Sedivy V, Joshi S, Ghaly Y, Mizera R, Zaloudikova M, Brennan S, Novotna J, Herget J, Gurney AM.** Role of Kv7 channels in responses of the pulmonary circulation to hypoxia. *Am J Physiol Lung Cell Mol Physiol* 308: L48-L57, 2015. doi: 10.1152/ajplung.00362.2013.

42. **Sitbon O.** HIV-related pulmonary arterial hypertension: clinical presentation and management. AIDS. 22 Suppl 3: S55-S62, 2008. doi: 10.1097/01.aids.0000327517.62665.ec

43. **Thibault HB, Kurtz B, Raher MJ, Shaik RS, Waxman A, Derumeaux G, Halpern EF, Bloch KD, Scherrer-Crosbie M.** Noninvasive assessment of murine pulmonary arterial pressure: validation and application to models of pulmonary hypertension. *Circ Cardiovasc Imaging* 3: 157-163, 2010. doi: 10.1161/CIRCIMAGING.109.887109.

44. **Triant VA.** Cardiovascular disease and HIV infection. *Curr HIV/AIDS Rep* 10: 199-206, 2013. doi: 10.1007/s11904-013-0168-6.

45. **Yuan JX, Aldinger AM, Juhaszova M, Wang J, Conte JV, Jr., Gaine SP, Orens JB, Rubin LJ.** Dysfunctional voltage-gated K+ channels in pulmonary artery smooth muscle cells of patients with primary pulmonary hypertension. *Circulation* 98: 1400-1406, 1998.

Figure captions

Fig.1. K^+ channel activity is reduced in PASMC from Tg26 mice. A: Representative current traces for 200 ms depolarization pulses from -60 mV to +20 mV in 10 mV increments from a holding potential of -60 mV in PASMC from Wt or Tg26 PA. B: Current-voltage relationships of K+ currents measured at the end of the pulse in myocytes from Wt (n=32 from 11 different animals) or Tg26 (n=26, from 9 different animals). C: Resting membrane potential values in PASMC from Wt (n=46 from 13 different animals) or Tg26 (n=40, from 12 different animals). *, and *** indicate $P < 0.05$ and $P< 0.001$ vs Wt; nested ANOVA.

Fig.2. Kv1.5 channel activity is not altered in PASMC from Tg26 mice. A and B: Representative current traces obtained when applying a depolarizing pulse to +20 mV before (black) and after (grey) the addition of the Kv1.5 channel blocker DPO-1 (10^{-6} M). Lower panel shows the current-voltage relationships of K^+ currents measured at the end of the pulse before and after the addition of DPO-1 in myocytes from Wt (n=7 from 6 different animals) or Tg26 (n=7, from 5 different animals), respectively. *and *** indicate $P < 0.05$ and $P< 0.001$ vs in the absence of DPO-1; nested ANOVA. C: Mean data of the DPO-1-sensitive currents obtained by subtracting the current in the absence and in the presence of the drug. D and E: Representative traces and averaged values of the contractile response induced by DPO-1 in PA from Wt and Tg26 mice. F and G: *KCNA5* mRNA expression by RT-PCR in Wt and Tg26 whole lung or PASMC homogenates, respectively. Results are means ± SEM of 4-5 samples, normalized by the expression of *ACTB*.

Fig.3. Loss of TASK currents in PASMC from HIV-1 Tg26. A and B: Ramp protocol and original I_{KN} recorded in PASMC from Wt or Tg26 mice. Representative traces recorded at pH 7.3 (black) and after changing to pH 6.3 (grey) are shown. B: Current-voltage relationships of the pH-

sensitive current obtained by measuring the difference in K^+ current at external pH values of 7.3 and 6.3 in PASMC from Wt (n=7 from 6 different animals) or Tg26 (n=7, from 5 different animals). C: Graph showing pH-sensitive current at 0 mV. ** indicate P < 0.01 vs Wt. D: Original recordings (D and E) of the effects of switching the pH of the external solution from 7.3 to 6.3 on membrane potential. F: Acid-induced membrane depolarization in PASMC from Wt or Tg26 mice (n=7 from 6 different animals) or Tg26 (n=8, from 5 different animals), respectively. *** indicate P < 0.001 vs Wt. F and H: Graphs show KCNK3 mRNA expression by RT-PCR in lungs or PASMC, respectively, from WT or Tg26 mice. Results are means ± SEM of 3-4 samples, normalized by the expression of *ACTB.*

Fig.4. Kv7 currents are reduced in PASMC from Tg26 mice. A: Representative current traces and current-voltage relationships of K^+ currents measured at the end of the 4s depolarization pulses from -60 mV to +20 mV in 10 mV increments from a holding potential of -60 mV in PASMC from Wt (n=31 from 14 different animals) or Tg26 (n=30, from 8 different animals). B: Representative current traces at +20 mV (B) and current-voltage relationships (C and D) of K^+ currents measured at the end of the pulse before and after the addition of the Kv7 channel blocker XE991 ($3x10^{-7}$ M) in myocytes from Wt (n=7 from 5 different animals) or Tg26 (n=6, from 5 different animals), respectively. *, ** and *** indicate P < 0.05, 0.01 and 0.001, respectively vs in the absence of XE991. E: Mean data of the XE991-sensitive currents obtained by subtracting the current in the absence and in the presence of the drug. *and ** indicate P < 0.05 and P< 0.01 vs Wt. Original recordings (F) and mean data (G and H) of the vasoconstriction induced by XE991 (n=5-7) and linopirdine (n=4-5), respectively. * and ** indicate P < 0.05 and P< 0.01 vs Wt.

649 Fig.5. Attenuated expression of and activity of Kv7.1 channels in PA from Tg26 mice. A: *KCNQ1,*
650 *KCNQ4* and *KCNQ5* mRNA expression by RT-PCR in Wt and Tg26 lungs. Results are means ±
651 SEM of 4-5 samples, normalized by the expression of *ACTB*. * indicates P<0.05 vs Wt. B and C:
652 Representative current traces at +20 mV and current density before and after the addition of
653 the Kv7.1 channel activator L364,373 (10^{-5} M) in PASMC from Wt (n=6, from 3 different
654 animals) and Tg26 mice (n=4, from 3 different animals), respectively. D and E: Original
655 recordings and mean data of the relaxation induced by L-364,373 in serotonin-stimulated PA
656 from Wt (n=8) or Tg26 (n=7). Results are means ± SEM. * indicate P < 0.05 vs Wt.
657
658 Fig 6. Electrophysiological and relaxant effects induced by retigabine. A and B: current density
659 at + 20 mV before and after the addition of the Kv7.2-Kv7.4 channel activator retigabine (10^{-5}
660 M) in PASMC from Wt (n=4, from 3 different animals) and Tg26 mice (n=4, from 3 different
661 animals), respectively. D and E: Original recordings and mean data of the relaxation induced by
662 retigabine in serotonin-stimulated PA from Wt (n=9) or Tg26 (n=8). Results are means ± SEM.
663
664 Fig. 7. Tg26 mice do not exhibit pulmonary hypertension A: Original recordings of pulmonary
665 arterial pressure in Wt (grey) and Tg26 (black) mice. B: Graphs showing means ± SEM of mean,
666 systolic and diastolic pulmonary arterial pressure (PAP), respectively, in Wt and Tg26 mice.
667 Results are means ± SEM (n=8-10). C and D: Graphs showing means ±SEM of right ventricular
668 systolic pressure (RVSP) and heart rate, respectively, in Wt and Tg26 mice. E: Right ventricular
669 (RV) weight relative to left ventricle + septum (LV+S) or to body weight (RV/BW), respectively.
670 Results are means ± SEM (n=10).
671
672 Fig. 8. Endothelial dependent relaxation is impaired in PA from HIV-1 Tg26 mice. A:
673 Vasoconstrictor responses induced by KCl. B: Original recordings and mean data (C) of the
674 vasoconstriction induced serotonin (5-HT). D and E: Relaxation induced by Acetylcholine (ACh)

675 or sodium nitroprusside (SNP), respectively in serotonin-stimulated PA. F: Relaxation induced
676 by Acetylcholine (Ach) in serotonin-stimulated mesenteric arteries. Results are means ± SEM. *
677 and ** indicate P<0.05 and P<0.01 versus Wt (n = 5-6 mice per group).
678
679 Fig. 9. Tg26 mice exhibit a modest pulmonary vascular remodeling. A: Representative
680 hematoxylin and eosin staining of paraffin-embedded lung sections from the Wt and Tg26
681 mice. B: Percentage of muscular, partially muscular and non-muscular PA in Wt and Tg26 mice.
682 C: Representative photomicrographs of elastica Van Gieson staining. D: % wall thickness of
683 pulmonary vessels in Wt and Tg26 mice (n = 4 per group). A total of 495-500 vessels were
684 measured per group. Scale bars = 50 µm.
685

686 Table 1. List of primers used.

Primer Name	Assay ID	Forward (5'-3)	Reverse (5´-3´)
HIV-1 Transgene		**TCCAGTTTGGAAAGGACCAG**	**TTGCCACACAATCATCACCT**
Positive control		**CTCCCAACCCCAGAGGTAGT**	**AGACCCCAGATCCAGAAAGG**
KCNA5	Mm00524346_s1		
KCNK3	Mm04213388_s1		
KCNQ1	Mm00434640_s1		
KCNQ4	Mm01185500_m1		
KCNQ5	Mm00524346_s1		
Actb	Mm02619580_g1		
NOS3		**GGTATTTGATGCTCGGGACT**	**TGTGGTTACAGATGTAGGTGAACA**
BMPR2		**GAGCCCTCCCTTGACCTG**	**GTATCGACCCCGTCCAATC**

687

688

689

690 Table 2. Noninvasive estimation of hemodynamic parameters in Wt and Tg26 mice by Doppler

691 echocardiography.

	Wt	**Tg26**
PAT, ms	16.53 ± 1.03	16.53 ± 0.21
ET, ms	57.41 ± 2.04	61.76 ± 1.99
PAT/ET (%)	28.98 ± 2.03	26.88 ± 0.78
TAPSE (cm)	10,5 ± 0.5	10,5 ± 1

692

693

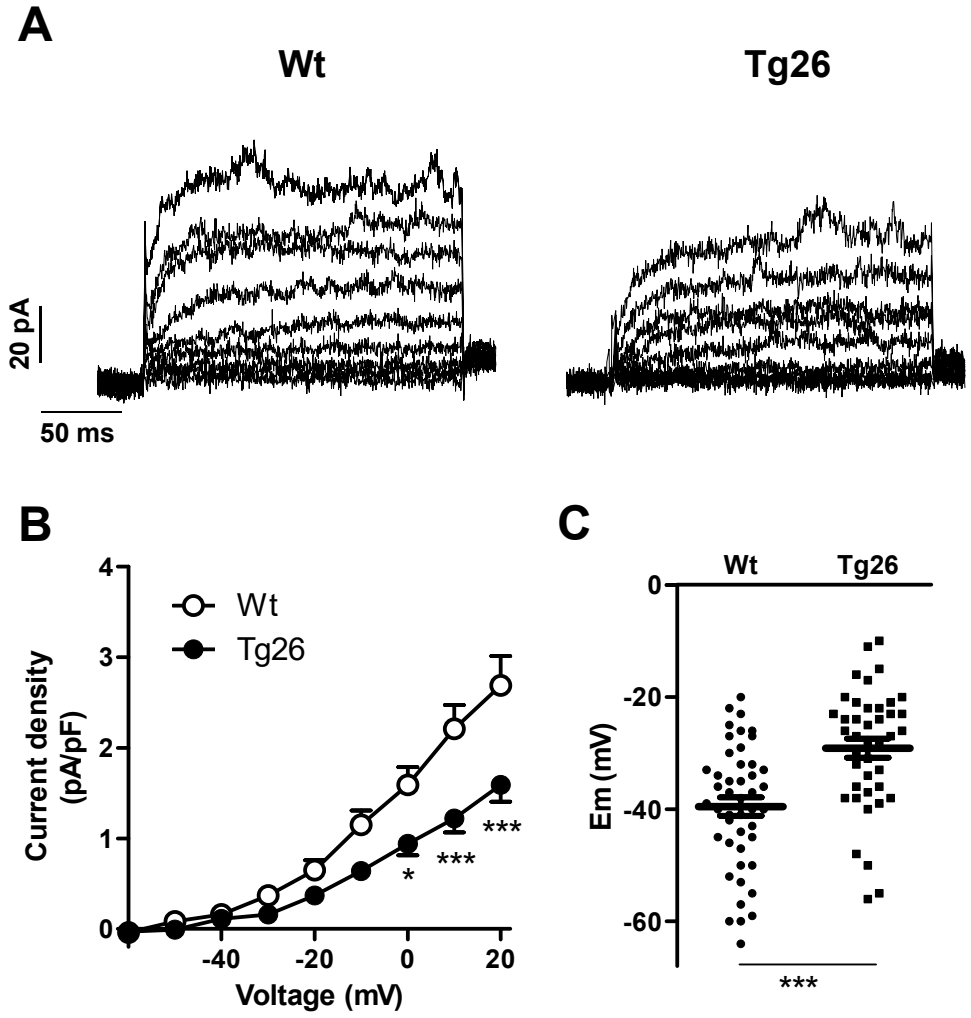
A
Wt
Tg26
20 pA
50 ms
B
Wt
Tg26
Current density (pA/pF)
Voltage (mV)
4
3
2
1
0
-40
-20
0
20
*
***
***
C
Wt
Tg26
Em (mV)
0
-20
-40
-60
***

Figure 1

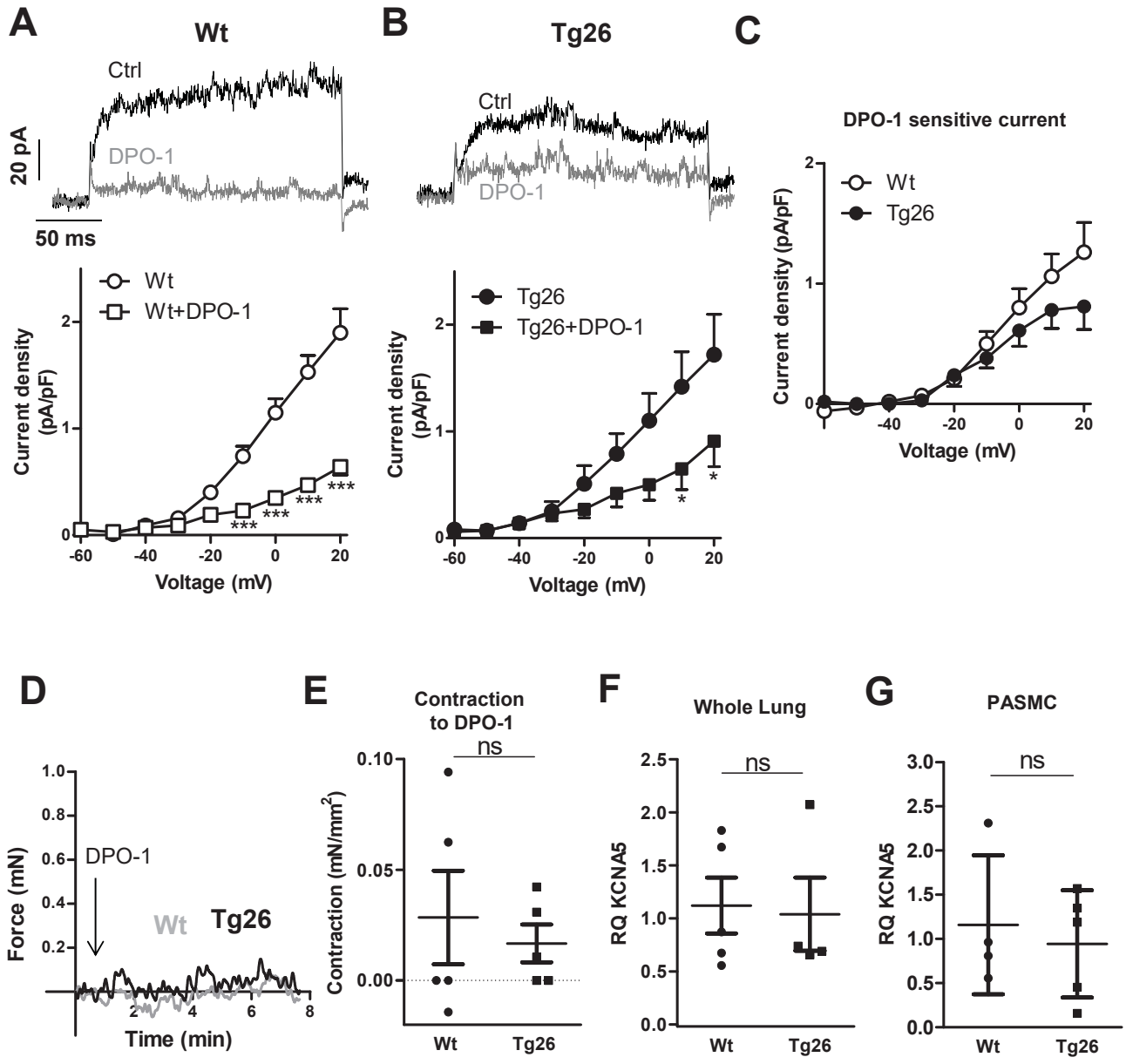
A
Wt
Ctrl
DPO-1
20 pA
50 ms
Wt
Wt+DPO-1
Current density (pA/pF)
Voltage (mV)
B
Tg26
Ctrl
DPO-1
Tg26
Tg26+DPO-1
Current density (pA/pF)
Voltage (mV)
C
DPO-1 sensitive current
Wt
Tg26
Current density (pA/pF)
Voltage (mV)
D
DPO-1
Wt
Tg26
Force (mN)
Time (min)
E
Contraction to DPO-1
ns
Contraction (mN/mm2)
Wt
Tg26
F
Whole Lung
ns
RQ KCNA5
Wt
Tg26
G
PASMC
ns
RQ KCNA5
Wt
Tg26

Figure 2

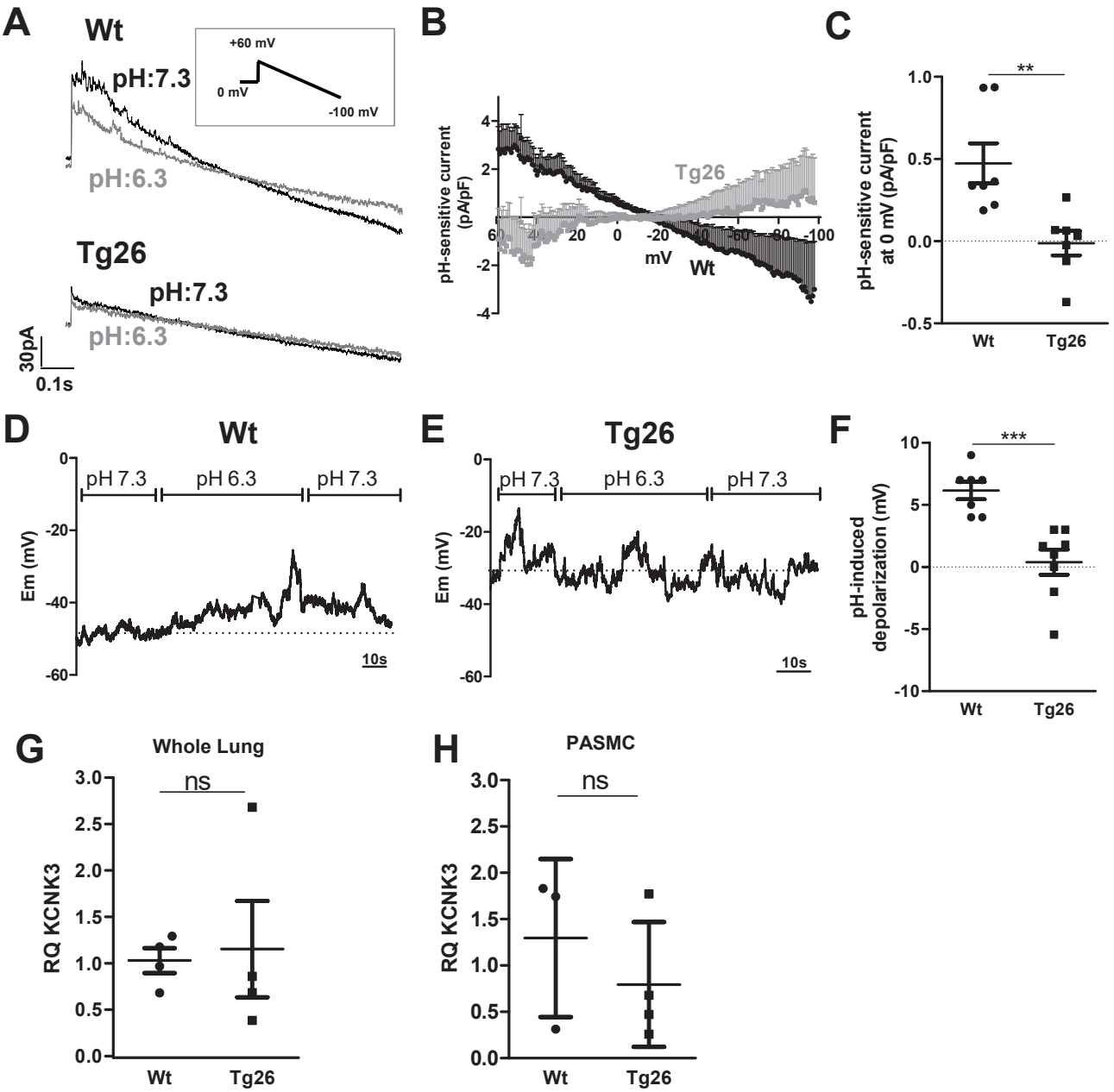
A
Wt
+60 mV
0 mV
-100 mV
pH:7.3
pH:6.3
Tg26
pH:7.3
pH:6.3
30pA
0.1s
B
pH-sensitive current (pA/pF)
Tg26
Wt
mV
C
pH-sensitive current at 0 mV (pA/pF)
**
Wt
Tg26
D
Wt
pH 7.3
pH 6.3
pH 7.3
Em (mV)
10s
E
Tg26
pH 7.3
pH 6.3
pH 7.3
Em (mV)
10s
F
pH-induced depolarization (mV)
***
Wt
Tg26
G
Whole Lung
ns
RQ KCNK3
Wt
Tg26
H
PASMC
ns
RQ KCNK3
Wt
Tg26

Figure 3

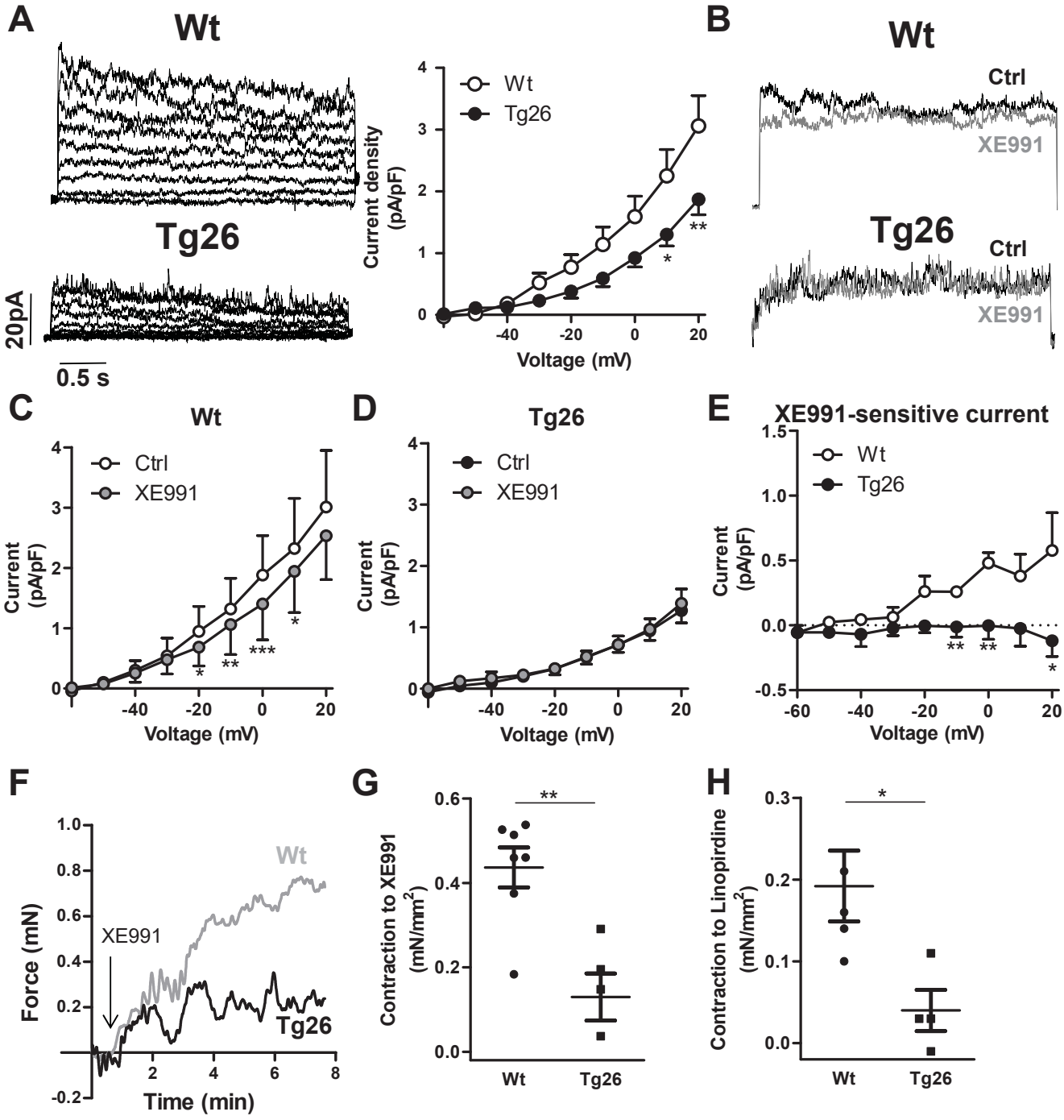
A
Wt
Tg26
20pA
0.5 s
Wt
Tg26
Current density (pA/pF)
Voltage (mV)
B
Wt
Ctrl
XE991
Tg26
Ctrl
XE991
C
Wt
Ctrl
XE991
Current (pA/pF)
Voltage (mV)
D
Tg26
Ctrl
XE991
Current (pA/pF)
Voltage (mV)
E
XE991-sensitive current
Wt
Tg26
Current (pA/pF)
Voltage (mV)
F
Wt
XE991
Tg26
Force (mN)
Time (min)
G
Contraction to XE991 (mN/mm2)
Wt
Tg26
H
Contraction to Linopirdine (mN/mm2)
Wt
Tg26

Figure 4

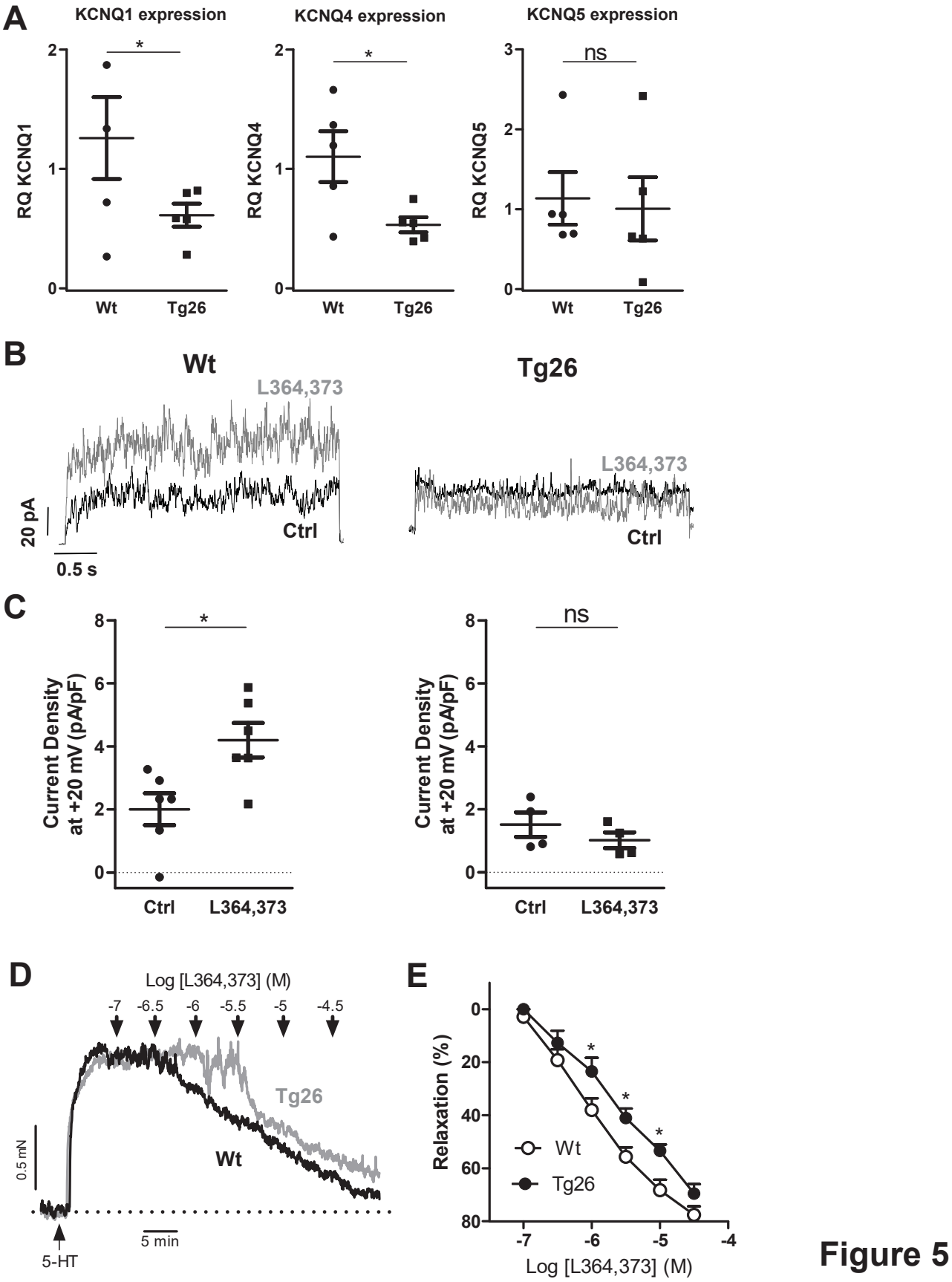
A
KCNQ1 expression
KCNQ4 expression
KCNQ5 expression
RQ KCNQ1
RQ KCNQ4
RQ KCNQ5
*
*
ns
Wt
Tg26
B
Wt
Tg26
L364,373
Ctrl
20 pA
0.5 s
C
Current Density at +20 mV (pA/pF)
Ctrl
L364,373
D
Log [L364,373] (M)
-7
-6.5
-6
-5.5
-5
-4.5
Tg26
Wt
0.5 mN
5 min
5-HT
E
Relaxation (%)
Wt
Tg26
Log [L364,373] (M)

Figure 5

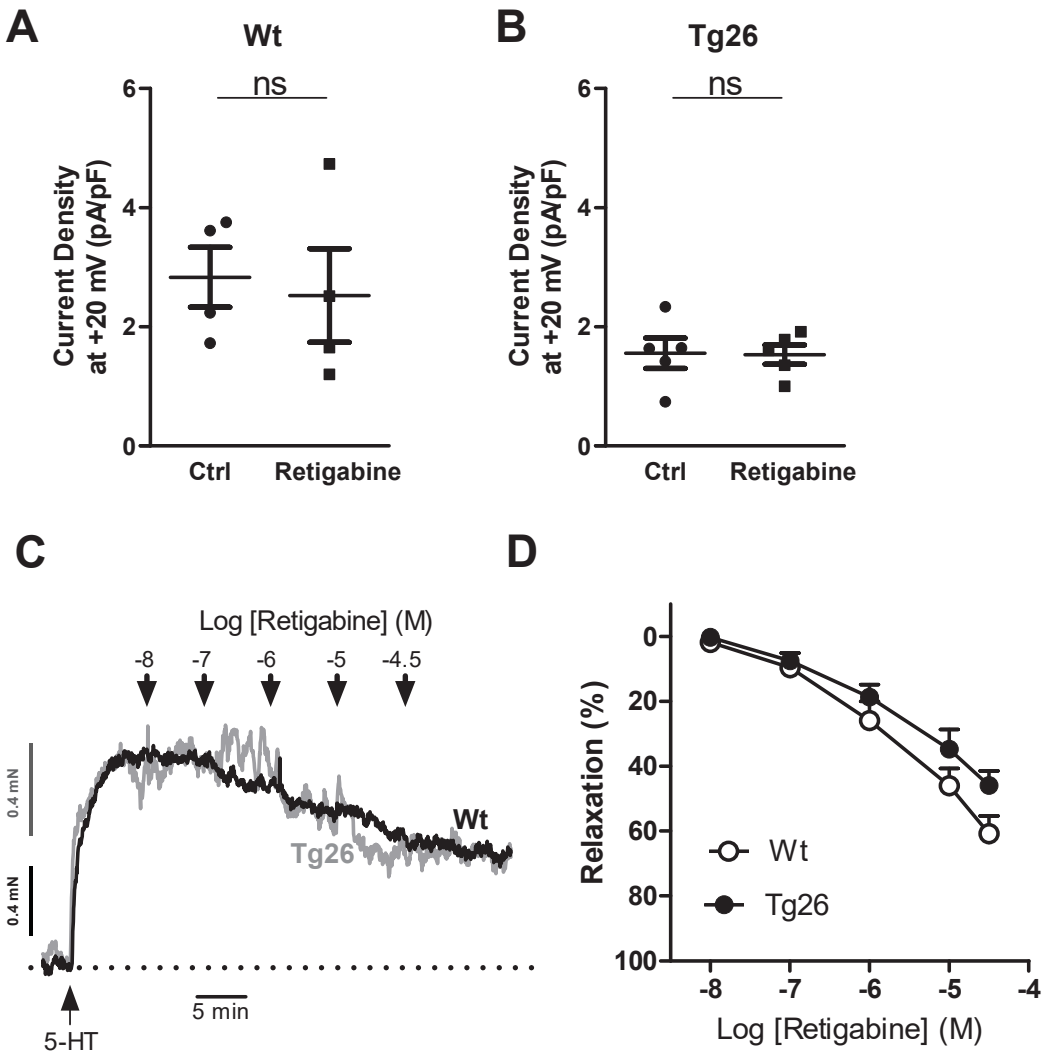
A
Wt
ns
Current Density at +20 mV (pA/pF)
6
4
2
0
Ctrl
Retigabine
B
Tg26
ns
Current Density at +20 mV (pA/pF)
6
4
2
0
Ctrl
Retigabine
C
Log [Retigabine] (M)
-8
-7
-6
-5
-4.5
0.4 mN
0.4 mN
Wt
Tg26
5 min
5-HT
D
Relaxation (%)
0
20
40
60
80
100
Wt
Tg26
-8
-7
-6
-5
-4
Log [Retigabine] (M)

Figure 6

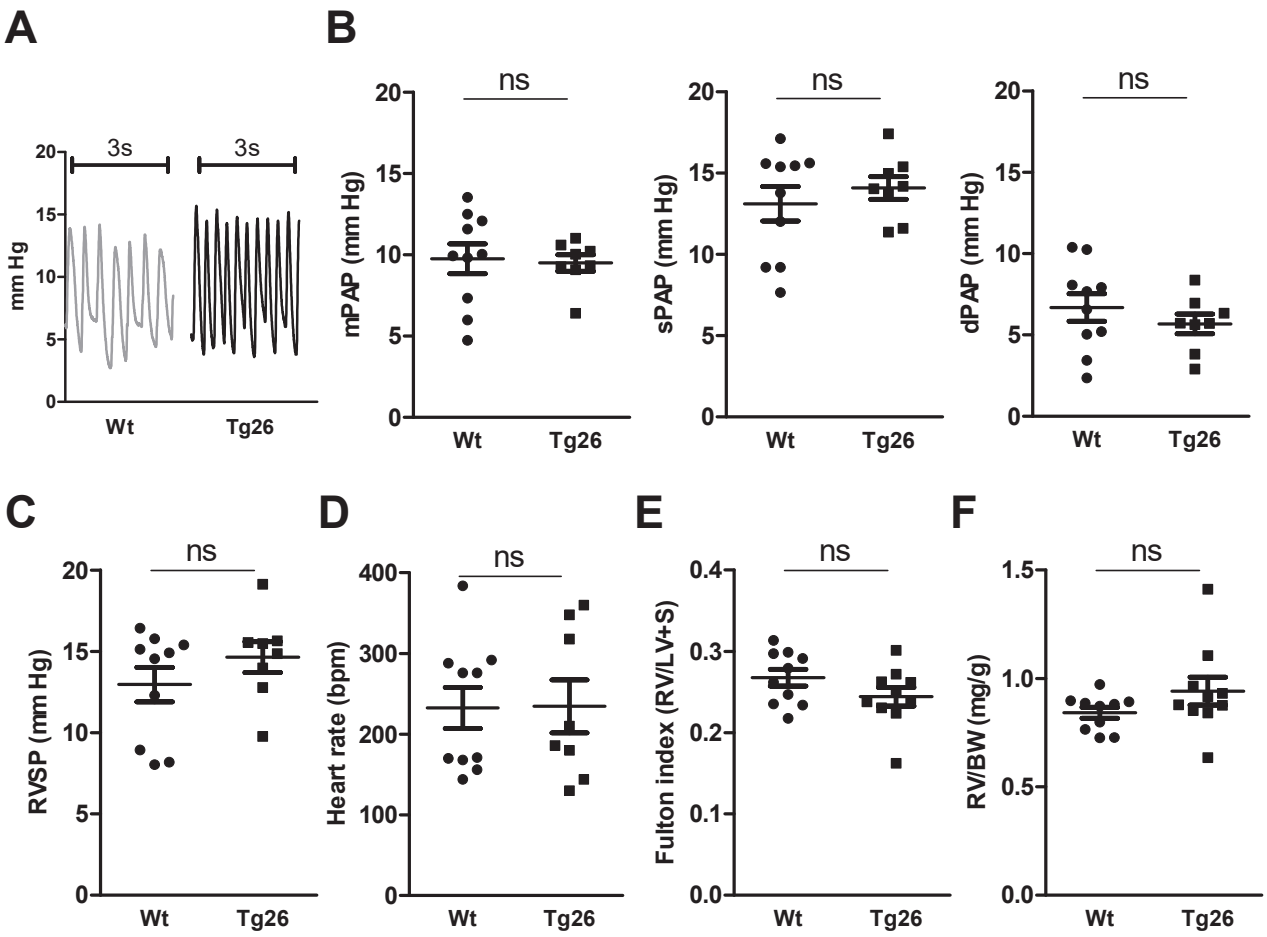
A
B
C
D
E
F
3s
3s
mm Hg
mPAP (mm Hg)
sPAP (mm Hg)
dPAP (mm Hg)
RVSP (mm Hg)
Heart rate (bpm)
Fulton index (RV/LV+S)
RV/BW (mg/g)
ns
Wt
Tg26

Figure 7

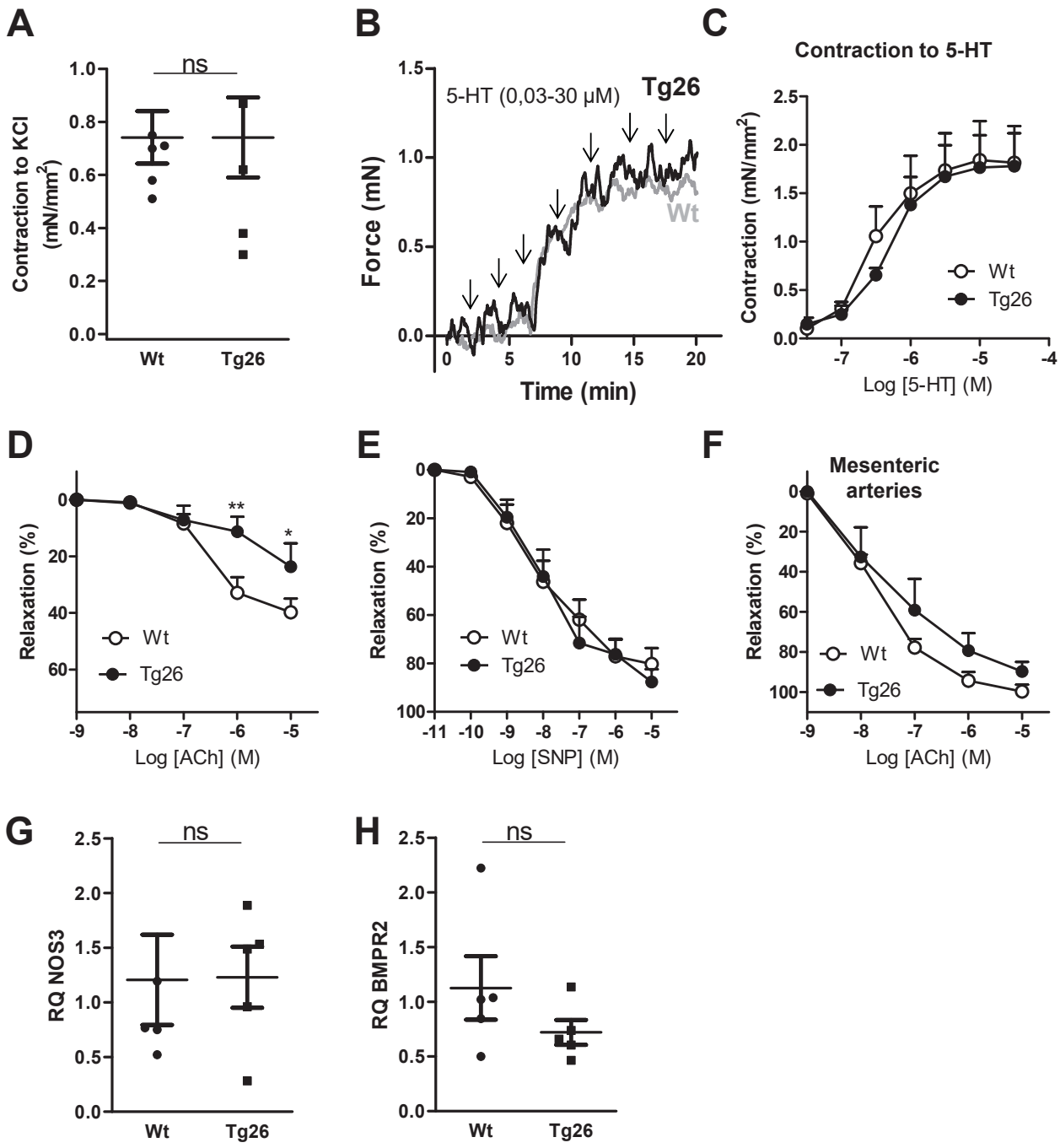
A
ns
Contraction to KCl (mN/mm²)
1.0
0.8
0.6
0.4
0.2
0.0
Wt
Tg26
B
5-HT (0,03-30 µM)
Tg26
Wt
Force (mN)
1.5
1.0
0.5
0.0
0
5
10
15
20
Time (min)
C
Contraction to 5-HT
Contraction (mN/mm²)
2.5
2.0
1.5
1.0
0.5
0.0
Wt
Tg26
-7
-6
-5
-4
Log [5-HT] (M)
D
Relaxation (%)
0
20
40
60
**
*
Wt
Tg26
-9
-8
-7
-6
-5
Log [ACh] (M)
E
Relaxation (%)
0
20
40
60
80
100
Wt
Tg26
-11
-10
-9
-8
-7
-6
-5
Log [SNP] (M)
F
Mesenteric arteries
Relaxation (%)
0
20
40
60
80
100
Wt
Tg26
-9
-8
-7
-6
-5
Log [ACh] (M)
G
ns
RQ NOS3
2.5
2.0
1.5
1.0
0.5
0.0
Wt
Tg26
H
ns
RQ BMPR2
2.5
2.0
1.5
1.0
0.5
0.0
Wt
Tg26

Figure 8

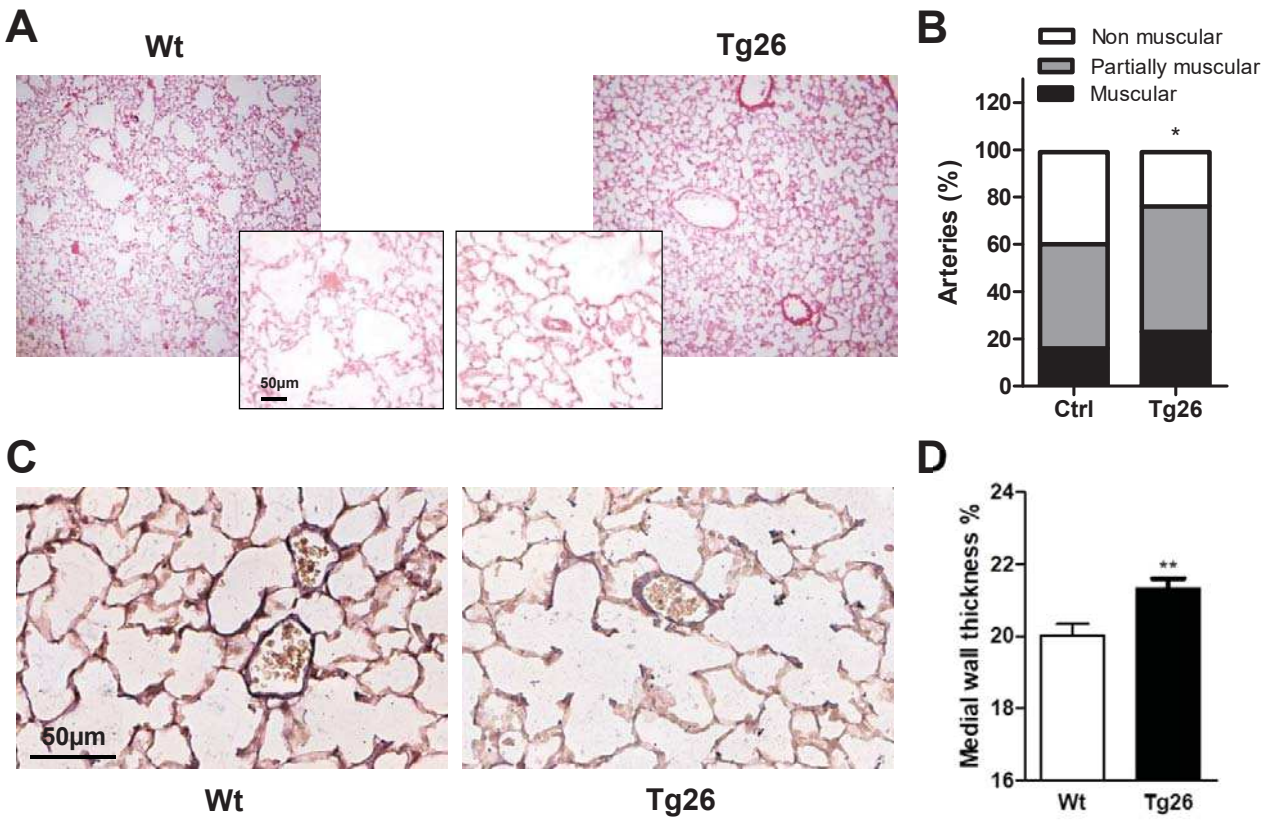
A
Wt
Tg26
50µm
B
Non muscular
Partially muscular
Muscular
Arteries (%)
120
100
80
60
40
20
0
*
Ctrl
Tg26
C
50µm
Wt
Tg26
D
Medial wall thickness %
24
22
20
18
16
**
Wt
Tg26

Figure 9